IRAS OBSERVATIONS OF Hα SELECTED EMISSION-LINE GALAXIES

M. REGO
Departamento de Astrofísica, Universidad Complutense, 28040 Madrid, Spain

M. CORDERO-GRACIA
ETSI Aeronaúticos, Universidad Politécnica, 28040 Madrid, Spain

J. ZAMORANO AND J. GALLEGO
Departamento de Astrofísica, Universidad Complutense, 28040 Madrid, Spain
Received 1 May 1992; revised 27 July 1992

ABSTRACT

We present the results of *IRAS* observations of the UCM (Universidad Complutense de Madrid) sample of emission-line galaxies, which have been selected from wide-dispersion Hα objective-prism plates. These data are intended to provide a convenient summary of the relevant far-infrared (FIR) properties of these galaxies. Color–color diagrams, as interpreted by theoretical models, suggest that emission from UCM galaxies is mainly due to dust heated directly by photons emitted in active star-forming regions. Statistical analysis of some samples, including the *IRAS* minisurvey and blue-selected objective-prism samples, have been performed. Comparisons, based on FIR luminosity distributions, with the *IRAS* minisurvey make evident the lower metallicity of the UCM galaxies which cannot be considered as a parent population of *IRAS*-detected galaxies. The FIR luminosity distributions of different samples have been compared using nonparametric methods and the best correlation has been found for the UCM and Wasilewski samples. Finally, a more detailed analysis of a UCM subsample has been performed from a three component model in order to get information concerning the fractional contribution of disk, star formation activity, and nonthermal mechanisms operating in the UCM galaxies.

1. INTRODUCTION

Surveys at optical wavelengths have been carried out with objective-prisms over the past several years. During the course of such surveys active galactic nuclei, quasars, and a large fraction of galaxies with strong star formation have been found, providing much of what we know about galaxy activity and induced star formation. Since most of the stellar energy output is re-emitted in the far infrared due to the thermal emission of interstellar dust heated by ultraviolet photons, any study of these optically-selected samples must take into account the far-infrared properties. At present it is clear from previous investigations, that emission from nonactive galaxies in the far infrared is due to the existence of at least two processes. The first converts the incident radiation field from high-energy photons to far-infrared (FIR) photons and the second involves the general interstellar radiation field. The FIR emission is related to the intensity and spectrum of the radiation field in which dust is embedded. Therefore, it is possible to acquire information about dust content and, consequently, on the metallicity from FIR observations.

The uniformity and extensive coverage of the *IRAS* survey make it well-suited to perform statistical studies on the FIR properties of different samples of galaxies. These analyses, when applied to several samples of optically-selected emission-line galaxies (ELGs), are useful in better understanding the distinctive physical processes taking place in these objects and to obtain information about the selection biases.

In this work, we focus on the UCM survey, which is being performed at the German–Spanish Observatory (Calar–Alto, Almería) with the Schmidt Telescope and a 4° objective prism, which provides a reciprocal dispersion of 1950 Å/mm at Hα. The conjunction of hypersensitized IIIaF emulsion with RG630 filter defines a spectral coverage from $\lambda\lambda$ 6400 to 6850 Å, which is able to record Hα emission in galaxies with a redshift up to $z=0.04$. Each plate covers a $5.5\times5.5°$ field in 24-cm-wide plates. Details about the detection techniques and first results can be found in Rego *et al.* (1989) and Zamorano *et al.* (1990). The sample of ELGs chosen for this study consists of 254 objects from the UCM objective-prism survey.

In this paper the UCM sample is initially compared with a prime sample containing normal, starburst, and Seyfert galaxies selected from the literature on the basis of their *IRAS* quality fluxes. Color–color diagrams obtained by plotting $\log(F_{25}/F_{60})$ and $\log(F_{60}/F_{100})$ are interpreted from a simple two temperature model and used to investigate the FIR properties. A statistical comparative study including the *IRAS* minisurvey (Carico *et al.* 1986) the UCM, University of Michigan (UM) (MacAlpine & Williams 1981), and Wasilewski (1983) samples is also carried out using the redshift and the FIR luminosities (LFIR) distributions. Finally, UCM galaxies with the best quality *IRAS* data have been selected in order to establish the fractions of disk, starburst, and power-law emission contributing to the observed fluxes.

2. *IRAS* OBSERVATIONS

As a first approach to study the far-infrared characteristics of the UCM ELGs sample, we searched the *IRAS Point Source Catalogue* (*PSC*) version 2.0 (Lonsdale *et al.* 1989) for position coincidences between the UCM galaxies and *IRAS* sources. A circular window of 4 arcmin centered on each object in our sample was employed; an additional flux condition of F_{25}/F_{60} was imposed in order to reject stellar sources. A total of 88 *IRAS* counterparts were found in the 282 search areas. The facilities of the Infrared Processing and Analysis Center (IPAC) at the Rutherford Appleton Laboratory (Oxford, England) were used for coadding the original *IRAS* scans data at the locations of each galaxy in our sample in order to detect a substantial number of additional sources. Since the UCM galaxies are virtually point sources as seen by *IRAS*, the data were coadded in a one-dimensional sense only.

After this second attempt a final sample of *IRAS*-detected UCM ELGs including 254 objects was obtained. The observational data are given in Table 1. The *IRAS* flux densities in Janskys are listed in columns 2 to 5. The photographic magnitudes and 143 redshifts available, measured from our own spectroscopic observations or extracted from the *Catalogue of Principal Galaxies* (Paturel *et al.* 1989), are provided in columns 6 and 7, respectively. Finally, column 8 contains alternate designations for the UCM galaxies that are found in other galaxy catalogs. The abbreviations refer to the following catalogs or surveys: CG= Pesch *et al.* (1991); HOLM=Holmberg (1937); KARA=Karachentsev (1972); KAZ=Kazarian & Kazarian (1980); KUG=KISO (Takase & Hiyauchi-Isobe 1991); M=Vorontsov-Velyaminov & Krasnogorskaja (1962); MK=Markarian & Lipovetskii, (1971, 1972, 1973, 1974, 1979); N=NGC (Dreyer 1888); PG =Palomar Green (Green *et al.* 1986); REIZ=Reiz (1941); U=UGC (Nilson 1973); UM=University of Michigan Survey (MacAlpine & Williams 1981); WAS =Wasilewski (1983) and ZWG=Zwicky & Herzog (1963).

3. FLUX PROPERTIES

It is of interest to examine the far-infrared properties of the UCM sample and to make comparisons with other galaxies. Therefore, we collected from the literature *IRAS* data corresponding to normal, starburst, and Seyfert 1 and 2 galaxies on the basis of their *IRAS* quality fluxes. It should be noted that these galaxies belong to distinct samples which have been selected with different criteria. However, for the purposes of this analysis the derived results do not lose generality by this constraint.

The reference sample contains 546 objects. Normal galaxies are represented by 229 objects which were selected mainly from the list of Devreux *et al.* (1987). We used 144 starburst galaxies from Balzano (1983), Kunth & Sargent (1983), Klein *et al.* (1984), Zotti *et al.* (1988), and Xu & De Zotti (1989). All Seyfert galaxies, including types 1 and 2, listed by Dahari & de Robertis (1988) were selected. This sample contains 81 Seyfert 1 and 92 Seyfert 2 galaxies, classified following the Veron Catalog (Venon-Cetty & Venon 1991).

A picture from Natta & Panagia (1976) shows the 12 and 25 μm emission coming from hot dust located in, or at least very near, H II regions. In this description the 60 and 100 μm emissions would be dominated by cooler dust associated with neutral gas outside of the ionized gas region (Thronson & Price 1982). The latter component could be located in shells surrounding the H II regions or in the associated neutral molecular gas clouds from which the H II region has formed (McBreen *et al.* 1982). In this analysis we exclude the 12 μm fluxes because of their higher uncertainties in most of the galaxies of the sample, and we concentrate on the F_{25}/F_{60} and F_{60}/F_{100} ratios. As Desert (1986) shows, these ratios can be generated assuming components which are subjected to increasingly intense radiation fields.

After excluding outliers, the first, Q1, and third, Q3, quartiles of the remainder sample were obtained. These quartiles, containing 50% of all observations, were used to define a domain on the diagram $\log(F_{25}/F_{60})$ vs $\log(F_{60}/F_{100})$ characterized by the higher frequency of each galaxy category. The normal galaxy sample inside the corresponding boundary has a mean value of -0.88 ± 0.13 for $\log(F_{25}/F_{60})$ and -0.39 ± 0.11 for $\log(F_{60}/F_{100})$. In the starburst case the estimated mean values for both ratios are respectively -0.70 ± 0.19 and -0.20 ± 0.09. The Seyfert galaxies exhibit $\log(F_{25}/F_{60})$ and $\log(F_{60}/F_{100})$ mean values of -0.44 ± 0.23 and -0.19 ± 0.16.

The same procedure was carried out for the UCM galaxies yielding estimated mean values of the $\log(F_{25}/F_{60})$ and $\log(F_{60}/F_{100})$ ratios of -0.65 ± 0.23 and -0.27 ±0.18. The subsample obtained in this way rejects UCM galaxies with upper limits and high uncertainties in *IRAS* fluxes and gathers the *IRAS* counterparts of the brightest UCM galaxies. This selection process is consistent with the objective-prism one, since the LFIR values, obtained as a combination of the 60 and 100 μm fluxes, are reasonably well correlated with the Hα luminosities as Dennefeld *et al.* (1985) have shown. It is appropriate to note that no attempt at completeness was made in assembling the subsample. Consequently, outside general statistical trends, no statement will be made about space densities or frequency of certain properties.

The loci defined by the Q1 and Q3 quartiles for each sample are plotted (Fig. 1), in a $\log(F_{25}/F_{60})$ vs $\log(F_{60}/F_{100})$ diagram. The UCM sample appears below the Seyfert area, between the starburst and normal galaxies regions. But the Seyfert and UCM galaxies coverage areas are significantly larger than those corresponding to normal and starburst galaxies. This spread can be due in the first case to the sample selection which include both Seyfert types 1 and 2, and in the second one, to the low-quality fluxes due to the faintness of most galaxies of the UCM sample. In summary, we conclude that the mean radiation field of UCM sample arises predominantly from dust heated by star-forming regions.

TABLE 1. UCM galaxy sample.

UCM	12μm	25μm	60μm	100μm	m_{pg}	z	Other names
UCM0000+2140	0.21	1.18	4.42	4.61	14.30	0.02170	MK334, U00006
UCM0001+2024	0.06	<0.06	<0.05	14.12	--	--	
UCM0003+1955	0.32	0.47	0.45	1.00	13.80	0.02560	MK335
UCM0003+2200	<0.05	<0.08	<0.10	0.55	16.50	--	KUG3+220
UCM0003+2215	<0.05	0.13	1.31	2.22	16	--	KAZ16
UCM0005+1802	<0.04	<0.05	0.09	<0.19	--	--	
UCM0006+2332	0.08	0.09	0.57	1.54	14.50	0.01510	N0009, U00078
UCM0009+2024	<0.05	<0.09	0.12	0.21	--	--	
UCM0009+2149	0.10	<0.04	<0.05	<0.23	--	--	
UCM0012+2109	<0.05	<0.08	<0.05	<0.16	--	--	
UCM0013+1944	<0.04	<0.05	0.15	0.41	--	--	
UCM0014+1748	0.10	0.21	1.10	1.72	14.90	0.01880	U00164
UCM0014+1829	<0.04	<0.08	0.24	0.43	--	0.01790	
UCM0015+2212	<0.03	<0.04	0.16	<0.26	16	0.01762	MK1141
UCM0017+1942	<0.03	0.07	<0.06	0.91	15.70	0.02589	ZWG457.004
UCM0017+2148	<0.05	<0.09	<0.13	<0.58	--	--	
UCM0018+2216	0.08	0.49	0.72	1.51	--	--	
UCM0018+2218	<0.04	<0.05	0.99	2.23	17	--	N0084
UCM0019+2201	<0.04	0.24	0.30	0.66	15.70	0.01980	ZWG479.012
UCM0022+2049	0.16	0.26	2.08	4.26	15.50	0.01840	ZWG457.013
UCM0023+1908	<0.04	0.12	0.29	0.75	--	--	
UCM0034+2120	<0.05	0.16	1.22	3.25	15.60	--	ZWG457.021
UCM0036+2007	<0.05	<0.10	<0.06	0.27	--	--	
UCM0037+2226	0.06	0.21	0.89	2.42	14.60	0.01959	U00425
UCM0038+0235	0.13	0.13	0.36	0.72	15.80	--	ZWG383.067
UCM0038+2259	0.12	0.16	0.25	0.86	--	--	
UCM0039+0050	<0.08	<0.09	<0.06	<0.19	15.60	--	ZWG383.070
UCM0040+0220	<0.04	0.18	0.20	0.33	17	--	UM063
UCM0040+0257	0.10	0.21	0.53	0.80	17	0.03755	MK1144, UM61
UCM0040+2312	0.09	0.08	0.75	2.23	15.80	0.02442	ZWG479.061
UCM0040-0023	<0.26	<0.38	1.78	4.55	13.60	0.01380	N0237, U00461
UCM0041+0135	0.11	0.15	0.27	0.74	14.20	0.00152	U00468
UCM0043+0245	0.07	0.12	<0.05	0.30	17	--	
UCM0043+2440	<0.05	0.10	0.17	<0.19	--	--	
UCM0043-0159	0.25	0.59	4.04	8.85	13.10	0.01359	MK555, U00476
UCM0044+2246	<0.04	0.08	0.45	0.60	16.90	--	M+04-03-003
UCM0045+2206	0.09	0.22	0.96	1.79	14.90	0.01940	MK347
UCM0045+2256	<0.05	<0.06	<0.08	0.18	--	--	
UCM0045-0304	0.05	0.41	0.24	0.40	15.30	--	HOLM022B
UCM0047+2051	0.05	0.09	0.61	1.41	--	--	
UCM0047+2413	0.10	0.30	2.06	3.38	15.50	0.03368	ZWG480.013
UCM0047+2414	<0.06	0.24	2.44	3.63	15.20	0.03379	ZWG480.014
UCM0047-0213	<0.04	<0.10	0.37	0.67	15.50	--	UM280
UCM0049+0017	<0.05	<0.07	0.20	0.45	17	0.01500	UM283
UCM0049-0006	<0.04	0.24	0.12	<0.16	18	--	UM282
UCM0050+0005	<0.06	0.23	0.30	0.33	16	0.03400	UM290
UCM0050+2114	0.10	0.38	1.99	2.64	14.50	0.02311	MK349
UCM0051+2430	0.09	0.13	1.11	1.59	15.10	--	U00547
UCM0053+2352	<0.05	<0.06	<0.06	<0.16	15.50	--	ZWG480.021
UCM0054+2337	<0.05	0.19	0.16	0.42	15.10	0.01700	MK350, U00591
UCM0054-0133	0.12	0.73	0.82	1.30	15.50	--	ZWG384.040
UCM0056+0043	0.09	<0.15	0.34	<0.23	16.60	0.01800	UM296
UCM0056+0044	<0.04	<0.09	0.26	0.22	17	--	UM295
UCM0118+2156	0.05	0.08	0.47	1.29	--	--	
UCM0121+2137	<0.04	<0.06	0.30	1.35	15.90	0.03389	ZWG481.007
UCM0129+2109	<0.05	0.23	1.30	2.46	14.80	--	U01098
UCM0134+2258	0.04	0.35	0.47	1.20	17	--	M+04-04-015
UCM0135+2242	0.05	<0.05	0.11	0.90	--	0.03600	
UCM0138+2216	0.12	0.14	0.44	1.72	--	--	
UCM0139+2226	0.11	<0.07	<0.10	0.57	15.50	0.04436	U01188
UCM0141+2220	<0.05	<0.06	0.38	0.66	--	--	
UCM0142+2137	<0.05	0.25	0.59	0.93	15.20	0.03503	ZWG482.008
UCM0145+2519	<0.06	<0.08	0.48	1.32	15.20	0.04086	ZWG482.015
UCM0147+2309	0.05	0.13	0.21	0.33	--	0.01900	
UCM0148+2124	0.06	<0.06	0.25	<0.19	--	0.01670	
UCM0150+2032	<0.05	0.06	0.10	0.34	--	0.03220	
UCM0150+2056	<0.05	0.16	<0.08	0.30	--	--	
UCM0152+2039	0.05	<0.05	0.07	0.24	--	--	
UCM0155+2223	<0.05	<0.07	<0.06	<0.16	--	0.02060	
UCM0155+2507	0.21	0.67	5.86	9.46	14.30	0.01642	U01451
UCM0156+2410	<0.05	<0.08	0.21	<0.19	14.80	0.01300	ZWG482.035
UCM0157+2102	<0.04	<0.07	0.60	0.98	14.30	0.01017	U01490
UCM0157+2324	0.13	0.25	1.34	3.38	13.30	0.01640	U01471, N0776
UCM0157+2413	0.08	0.20	1.43	2.61	14.90	--	U01479
UCM0158+2354	<0.04	<0.06	0.18	<0.16	--	0.01710	
UCM0159+2327	<0.04	0.13	0.42	0.81	15.50	0.01576	ZWG482.050
UCM0206+2300	0.15	0.08	0.65	1.01	--	0.02700	
UCM0206+2330	0.08	<0.06	<0.05	<0.16	--	--	
UCM0214+2404	<0.05	<0.07	0.42	0.69	--	--	
UCM0218+2322	<0.06	0.12	0.49	1.80	14.50	0.03149	U01808
UCM1246+2727	<0.04	0.09	0.13	0.25	15.50	0.02005	MK657, N4702
UCM1247+2701	<0.04	<0.04	0.10	0.31	16	0.02300	KUG1247+270
UCM1248+2911	<0.04	<0.05	0.42	1.43	15.20	0.02154	N4735
UCM1253+2756	0.07	<0.08	0.70	0.99	15.70	0.01651	MK53

TABLE 1. (continued)

UCM	12μm	25μm	60μm	100μm	m_{pg}	z	Other names	UCM	12μm	25μm	60μm	100μm	m_{pg}	z	Other names
UCM1253+2926	<0.03	0.08	0.06	0.30	--	--		UCM1313+2938	0.08	0.07	0.31	0.25	16.60	0.03709	WAS66
UCM1254+2740	0.07	0.17	0.22	0.62	15.90	0.01624	MK55	UCM1314+2827	<0.03	<0.04	0.15	<0.19	--	--	CG1001
UCM1254+2741	<0.03	<0.05	<0.05	<0.13	--	--		UCM1320+2727	<0.04	<0.05	0.12	0.19	--	--	CG1019
UCM1254+2802	<0.08	0.12	0.15	0.31	--	0.02000		UCM1321+2648	<0.04	<0.06	0.16	0.46	15.60	--	KUG1321+268
UCM1254+2853	0.08	<0.06	<0.06	0.32	--	--		UCM1324+2650	0.08	0.18	0.66	1.01	15.20	0.02356	KUG1324+268
UCM1254+2932	<0.05	<0.08	<0.06	<0.16	--	--		UCM1324+2926	<0.05	0.08	<0.08	0.18	--	--	WAS70
UCM1255+2734	0.07	0.10	0.39	0.61	16.50	0.02491	KUG1255+275	UCM1331+2901	<0.04	<0.04	<0.05	<0.16	17.40	0.03520	WAS74
UCM1255+2819	<0.05	0.37	0.31	0.41	15.90	0.02718	KUG1255+283	UCM1428+2727	<0.03	0.09	0.76	1.24	15.30	0.01490	KUG1428+274
UCM1255+3125	<0.04	0.12	0.26	0.48	15.50	0.02521	WAS064	UCM1429+2645	<0.03	<0.04	<0.06	0.33	--	--	
UCM1256+2702	0.07	<0.07	<0.08	<0.23	--	0.02300		UCM1430+2947	0.05	0.19	0.49	1.09	--	0.02900	
UCM1256+2722	<0.03	<0.08	0.23	0.84	--	0.02600		UCM1431+2702	0.10	0.13	0.19	0.36	--	0.03900	
UCM1256+2732	0.08	<0.05	0.34	0.36	15.60	0.02457	MK56	UCM1431+2814	<0.03	<0.05	0.09	0.21	--	0.02900	
UCM1256+2754	0.06	0.15	0.40	0.65	15.10	0.01835	MK58	UCM1431+2854	0.07	<0.03	0.26	0.61	15.50	0.02900	ZWG163.078
UCM1256+2823	0.06	0.18	0.44	1.02	15.70	0.03131	N4858	UCM1431+2947	0.05	<0.04	<0.05	<0.13	--	0.02000	
UCM1256+2910	<0.04	<0.07	<0.08	0.38	--	0.02500		UCM1432+2645	0.22	0.13	0.53	1.33	15.20	--	U9384
UCM1257+2754	0.06	0.22	0.13	0.29	--	--	PG1257+279	UCM1439+2439	0.10	0.08	0.13	0.29	--	--	
UCM1257+2808	<0.04	<0.06	0.35	0.36	16.10	0.01709	MK60	UCM1440+2511	0.17	<0.17	<0.14	0.20	--	--	
UCM1257+2825	<0.04	0.14	0.11	0.36	--	--		UCM1440+2521	0.06	0.07	0.43	1.12	15.90	0.02600	U9489
UCM1258+2754	<0.04	0.12	0.23	0.23	15.50	0.02492	ZWG160.086	UCM1441+2918	0.04	<0.04	0.08	0.23	14.90	--	REIZ4327
UCM1259+2755	0.09	0.16	0.64	1.09	15.10	0.02398	N4926A	UCM1442+2845	<0.02	0.12	0.46	0.68	14.90	0.01100	ZWG164.015
UCM1259+2934	0.26	1.31	6.61	7.10	13.90	0.02380	N4922B, U8135	UCM1443+2548	0.07	0.07	0.65	0.90	15.40	--	ZWG134.030
UCM1259+3011	0.05	<0.05	0.25	0.53	--	--		UCM1443+2714	0.16	0.34	0.78	1.22	15.40	0.02930	ZWG164.019
UCM1300+2907	<0.05	<0.05	<0.06	<0.13	--	0.02300	CG963	UCM1443+2844	<0.04	0.05	0.55	1.29	15.60	0.02800	ZWG164.021
UCM1300+3136	0.52	0.41	<0.06	0.24	--	--		UCM1444+2923	<0.03	<0.03	<0.05	<0.10	--	0.02400	
UCM1301+2904	<0.04	0.09	0.17	0.54	15.30	0.02682	KUG1301+290, ZWG160.128	UCM1445+2855	0.05	<0.03	0.05	<0.13	--	--	
UCM1301+3000	0.06	<0.07	0.09	0.19	--	--		UCM1447+2535	<0.03	0.08	0.29	0.67	14.60	0.03390	U9544
UCM1302+2853	<0.05	0.07	0.20	0.55	16	--	KUG1302+288A, CG968	UCM1449+2843	<0.05	0.10	<0.06	0.45	15.70	--	ZWG164.035
UCM1302+3032	<0.04	<0.04	0.07	<0.13	17	0.03328	MK62	UCM1449+2847	0.05	<0.03	<0.05	0.33	--	0.01600	
UCM1303+2908	0.05	0.06	0.12	<0.16	--	0.02600	CG972	UCM1451+2954	0.05	<0.04	<0.05	<0.10	--	--	
UCM1304+2808	0.31	<0.09	0.98	1.87	15	--	KUG1304+281	UCM1452+2754	<0.03	0.06	0.25	0.59	--	0.03200	
UCM1304+2818	<0.03	<0.05	<0.08	0.64	15.60	0.02431	KUG1304+283, ZWG160.141	UCM1506+1924	0.06	0.14	11.51	15.60	--	--	ZWG106.006
UCM1304+2830	<0.03	<0.05	<0.03	<0.19	--	0.02000		UCM1513+2012	0.08	0.48	3.01	3.81	15.60	0.03300	ZWG106.023
UCM1304+2848	<0.03	0.06	0.10	<0.13	14.70	0.02132	N4971	UCM1537+2506	0.20	0.51	2.37	3.11	15.50	0.02285	ZWG136.042
UCM1306+2937	<0.03	0.14	0.61	1.30	15.10	0.02088	KUG1306+296	UCM1557+1423	0.05	0.08	0.16	0.40	--	--	
UCM1306+3100	<0.04	<0.03	<0.06	0.32	--	0.02100		UCM1604+1642	0.13	<0.06	0.16	0.79	--	--	
UCM1307+2910	0.12	0.10	0.90	2.47	13.90	0.01869	N5000, U08241	UCM1612+1309	0.04	0.12	0.09	0.32	--	0.01100	
UCM1307+3111	<0.05	<0.08	0.16	0.39	--	0.01500		UCM1646+2725	<0.04	<0.06	<0.08	1.02	--	--	
UCM1308+2950	0.08	0.23	2.12	3.64	15	0.02420	N5004C, U08259	UCM1647+2727	<0.03	<0.04	0.25	1.04	--	--	
UCM1308+2958	<0.06	0.08	0.21	0.79	15.30	0.02125	N5004B	UCM1647+2729	0.06	<0.06	0.23	<0.58	15.60	--	KUG1647+274
UCM1310+3027	<0.05	0.25	0.17	0.33	--	0.01800		UCM1647+2950	0.10	0.13	0.79	1.57	15.30	0.02900	KUG1647+298
UCM1312+2954	0.09	0.10	0.40	0.68	--	0.01800		UCM1648+2855	0.04	0.18	0.66	1.70	15	0.03080	MK1108
UCM1312+3039	0.10	0.19	1.02	1.99	15.40	0.02100	ZWG160.170	UCM1651+3017	0.04	<0.02	<0.05	<0.16	--	--	

TABLE 1. (continued)

UCM	12μm	25μm	60μm	100μm	m_{pg}	z	Other names
UCM1653+2644	0.49	0.74	0.65	6.59	14.70	0.03453	U10607
UCM1654+2812	<0.03	<0.03	<0.05	0.30	--	--	
UCM1655+2755	<0.03	0.08	0.13	0.52	15.50	0.03380	N6264
UCM1656+2744	0.10	0.09	0.25	1.57	--	--	
UCM1656+2845	0.09	<0.04	0.11	0.31	--	--	
UCM1657+2900	<0.02	<0.05	0.21	0.56	--	0.03100	KUG1657+290
UCM1659+2928	0.07	0.04	0.12	0.77	16.10	0.03670	MK504
UCM1701+3131	0.08	0.25	2.12	3.54	15.40	0.03370	U10675
UCM2238+2308	<0.05	0.15	1.08	2.15	14.70	0.02383	U12148
UCM2239+1959	0.12	0.87	2.39	2.95	14.90	0.02375	KUG2239+199
UCM2239+2402	<0.05	<0.05	<0.06	0.43	--	--	
UCM2244+2049	<0.05	<0.05	<0.06	0.77	14.90	--	N7375
UCM2249+2149	<0.05	0.19	0.32	<0.36	--	--	
UCM2250+2427	0.19	0.81	3.46	4.91	15.40	0.04211	KUG2250+244
UCM2251+2352	<0.06	<0.09	0.25	0.61	--	0.02600	
UCM2253+2219	<0.05	0.15	0.51	0.59	--	0.02400	KUG2253+223
UCM2253+2453	<0.04	<0.07	<0.06	1.14	--	--	
UCM2255+1654	0.12	<0.07	0.70	1.67	--	0.03800	
UCM2255+1926	<0.04	0.07	<0.06	<0.23	--	0.01700	
UCM2255+1930	0.09	0.11	1.65	2.53	14.50	0.01894	U12265
UCM2256+2007	<0.05	0.13	0.44	1.21	15.50	--	ZWG453.037
UCM2257+2438	<0.05	0.13	0.45	2.12	16.80	0.03370	KAZ320
UCM2258+1920	<0.04	<0.05	0.32	<0.32	15.20	0.02200	ZWG453.046
UCM2300+2014	<0.03	0.14	0.42	0.36	--	--	
UCM2302+2053	0.11	<0.04	0.75	<0.64	--	--	
UCM2303+1702	<0.05	0.10	0.38	0.66	--	0.04200	
UCM2303+1856	0.10	0.49	2.29	2.18	15.70	--	ZWG453.067
UCM2304+1640	<0.04	<0.07	<0.10	<0.45	--	0.01500	
UCM2305+1621	0.04	0.05	0.22	<0.35	--	0.03600	
UCM2306+1703	0.06	0.08	0.13	1.28	--	--	
UCM2306+1947	0.23	0.10	<0.08	2.50	15.80	0.02600	KARA1007
UCM2307+2118	0.11	<0.05	<0.06	1.42	--	--	
UCM2310+1800	<0.04	0.11	0.44	1.37	--	--	
UCM2312+2204	0.06	0.08	0.20	0.66	--	--	
UCM2312+2500	0.27	0.13	0.13	1.65	14.40	0.02662	N7548, U12455
UCM2313+1842	<0.07	0.10	0.24	2.56	--	0.02900	
UCM2313+2516	0.24	2.00	10.41	11.16	15	0.02732	ZWG475.056
UCM2315+1625	0.08	0.08	<0.08	0.58	15.80	--	ZWG454.027
UCM2315+1658	<0.05	0.28	<0.06	<0.26	--	--	
UCM2315+1923	0.12	0.11	0.22	<0.48	--	--	
UCM2316+2028	<0.07	0.12	0.43	1.05	--	0.02620	
UCM2316+2457	0.24	0.62	4.22	7.05	14.10	0.02700	U12490
UCM2316+2459	<0.05	<0.06	2.44	6.14	15.70	--	KARA72.581B
UCM2317+1607	0.38	<0.07	0.10	<0.19	--	0.02000	
UCM2317+2356	0.18	0.31	2.72	5.85	13.60	0.03190	N7620,U12520
UCM2319+2234	<0.04	0.08	0.31	0.56	--	--	KUG2319+225
UCM2319+2243	0.09	0.07	0.13	0.53	--	--	
UCM2320+2428	0.17	0.18	0.56	1.43	15.70	--	ZWG476.027
UCM2321+1631	0.06	<0.06	<0.06	0.19	14.70	0.03842	N7647, U12576
UCM2321+2149	<0.03	<0.05	0.16	0.41	--	--	
UCM2321+2506	<0.05	0.26	0.41	0.67	15.10	0.03300	KUG2321+251
UCM2322+2218	0.09	<0.06	0.27	<0.19	--	0.02470	
UCM2323+2047	<0.04	<0.07	0.21	0.42	--	--	
UCM2323+2252	0.08	0.08	<0.05	<0.16	--	--	
UCM2324+2448	0.21	0.21	1.74	5.04	13.40	0.01240	N7664, U12598
UCM2325+1815	0.09	0.09	0.69	2.01	14.80	--	ZWG454.069
UCM2325+1945	<0.06	<0.05	0.41	0.66	15.60	--	ZWG454.070
UCM2325+2208	0.42	0.88	7.16	14.80	12.50	0.01162	N7678, U12614
UCM2325+2318	0.10	0.61	4.97	6.79	13.20	0.01140	N7673, U12607
UCM2326+2435	<0.05	0.16	1.00	2.08	--	0.01200	
UCM2327+1956	0.09	<0.04	0.11	0.37	15.50	--	U12641
UCM2327+2154	0.05	<0.06	<0.08	0.35	--	--	
UCM2327+2515	0.06	0.36	1.52	1.68	15	0.01911	ZWG476.055
UCM2328+2109	<0.04	0.06	0.14	0.80	15.70	--	ZWG455.003
UCM2329+2427	0.08	<0.05	0.19	0.43	15.70	0.01901	ZWG476.060
UCM2329+2447	0.04	<0.05	<0.10	0.46	--	--	
UCM2329+2500	0.07	0.06	0.10	0.79	15.60	0.02800	KAZ341
UCM2329+2511	<0.05	0.12	0.11	1.01	--	0.01340	
UCM2331+2214	0.08	0.06	0.10	0.44	--	0.03200	
UCM2332+1723	<0.04	<0.05	0.41	1.44	--	--	
UCM2332+1757	<0.04	<0.06	0.50	1.10	14.10	0.00465	U12682
UCM2333+2241	0.04	0.09	0.10	0.40	--	--	
UCM2333+2248	<0.07	<0.14	0.13	0.36	--	--	
UCM2333+2359	<0.05	<0.05	<0.08	0.48	--	0.03300	
UCM2334+2134	<0.07	<0.07	0.08	0.32	--	--	
UCM2348+2407	0.12	<0.07	<0.06	0.65	--	--	
UCM2351+2321	0.12	0.08	0.15	0.34	--	--	
UCM2352+2040	0.23	0.14	0.10	0.56	--	--	
UCM2357+2440	<0.05	0.15	<0.06	0.26	--	--	
UCM2358+2327	<0.05	<0.06	<0.06	0.50	--	--	

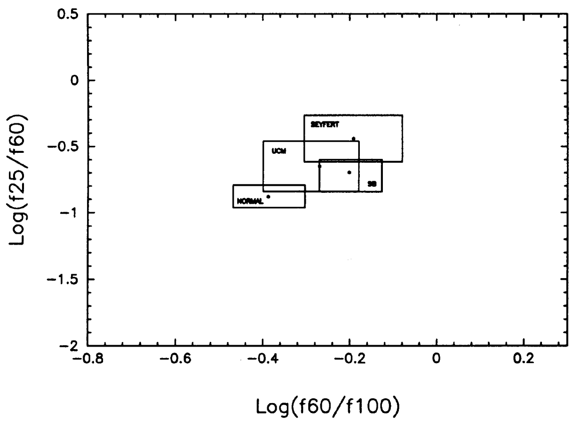

FIG. 1. The *IRAS* color–color diagram for normal, starburst, Seyfert, and UCM galaxies. Rectangles are defined by the Q1 and Q3 quartiles.

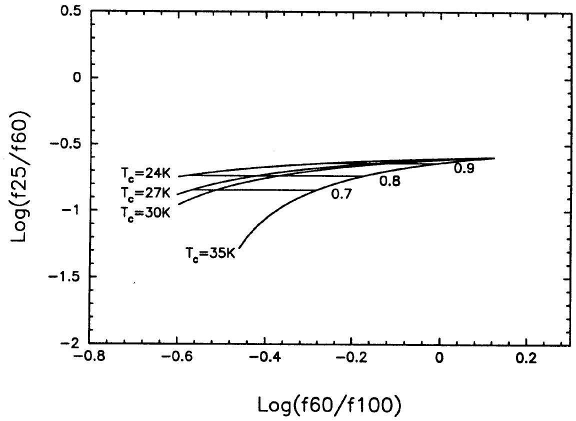

FIG. 2. *IRAS* color–color plot computed from the two component models assuming different cool temperatures.

4. THE TWO TEMPERATURE MODELS

The diagram of Fig. 1 can be interpreted, for the non-active galaxies, by a simple model. We adopt as our starting assumption, that the IR emission is predominantly thermal and the result of the contribution of two components. One is the radiation emitted by dust heated by blue photons provided by the stellar fields which is represented by a temperature T_c. The other component is the radiation produced by dust heated not only by blue photons, but also by UV ones emitted by the starburst nuclei. We assign a temperature T_w to this component which includes all the IR sources except the cool component. Following Sekiguchi (1987), we have constructed a model using T_w and the fraction of the warm-component contribution to the total 60 μm observed fluxes as indicators of the star formation activity degree. Introducing a T_c value, the model supplies the $\log(F_{25}/F_{60})$ and $\log(F_{60}/F_{100})$ ratios for a grid of T_w.

To choose a T_c value is a critical problem. Bothun *et al.* (1989) show, from a simplified model, that the disk temperature is a function of the ratio of UV-to-blue photons. In the absence of any UV heating photons, the Bothun model predicts an average temperature for the whole disk of 20 K, but in a disk where the UV and blue density of photons are equals (which occurs in a Sc galaxy) T_c would be 35 K. To illustrate the cool temperature effects on the two components model, we have plotted in Fig. 2 the $\log(F_{25}/F_{60})$ and $\log(F_{60}/F_{100})$ ratios, computed by assuming distinct T_c values ranging from 24 to 35 K, and a T_w fixed value of 90 K. For a given observed color, the predicted T_w and the fraction of the warm-component contribution to the total 60 μm, depends on T_c, as is shown in Fig. 2. Obviously, when objects placed in the left-hand region of the diagram are considered, a stronger dependence is found. Models with T_c values ranging from 24 to 30 K exhibit differences lower than 10% when an outermost observable $\log(F_{60}/F_{100})=-0.50$ ratio is considered. These discrepancies decrease when higher values are taken into account. The model constructed with a $T_c=35$ K shows the existence of an important fraction of UV photons in the disk temperature. The model grid was built adopting a mean value for T_c of 30 K, which remains fixed and a warm temperature network ranging from 80 to 110 K. Figure 3 displays the model features in the two color diagram, where the domains represented in Fig. 1 have been superimposed.

From the two-component model summary information about the UCM and the nonactive comparison samples can be extracted. The mean value of the normal galaxies sample is placed on the $T_w=83$ K curve with a fraction of 0.79 of the warm component to the total 60 μm fluxes, while the starburst sample appears around $T_w=87$ K and a fraction of 0.875. In the UCM case these values are $T_w=92$ K and 0.85. The Seyfert mean is located on the $T_w=108$ K curve. The T_w curve of the starburst is close to that of the UCM sample, confirming the starburst nature of most of these galaxies.

5. STATISTICAL ANALYSIS OF THE DATA BASE

In order to make known differential properties, it is suitable to compare the FIR properties of the UCM sample with those of the *IRAS* minisurvey, which represents a

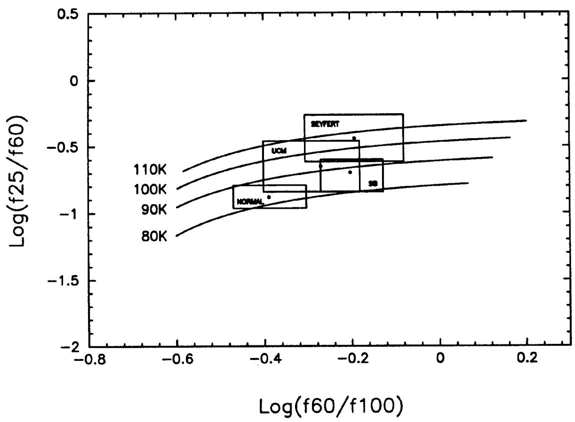

FIG. 3. Two-component model network assuming $T_c=30$ K superimposed on the observed domains of Fig. 1.

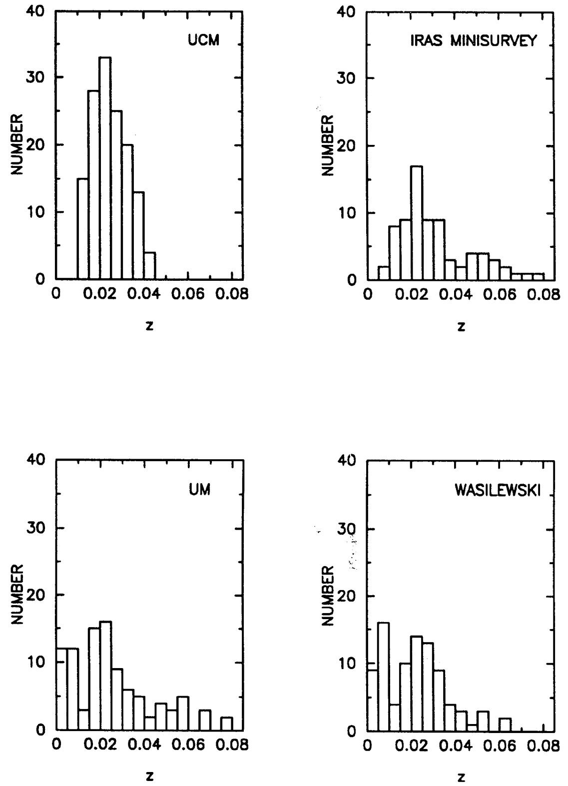

FIG. 4. Redshift distribution for the UCM sample compared with that seen in *IRAS* minisurvey, UM, and Wasilewski samples.

complete far-infrared selected sample of galaxies, and with two blue selected objective-prism samples: UM and Wasilewski collected from the studies of Salzer & MacAlpine (1988) and Bothun *et al.* (1989), respectively.

5.1 The Redshift Distributions

In Fig. 4 the redshift distribution for our UCM sample is compared with those obtained for *IRAS* minisurvey, UM, and Wasilewski. The redshift medians are 0.0241 for the UCM sample, 0.02575 for the *IRAS* minisurvey, and 0.0228 and 0.0215 for the UM and Wasilewski samples, respectively.

The *IRAS* minisurvey covers the A400–A539 supercluster complex which is at redshift $z=0.02$–0.03 (Geller *et al.* 1988) and the CrB supercluster which is at $z=0.07$. The Wasilewski sample overlaps the North Galactic Pole and is influenced by the Local Supercluster (Bothun *et al.* 1989) which also strongly affects the UM redshift distribution giving rise to a peak in the low-redshift region. The UCM redshift distribution peaks around $z=0.025$. This clumping in redshift reflects the coverage of the Coma supercluster. Therefore, these redshift distributions probably are more indicative of large structure than any sample selection effects.

5.2 The FIR Luminosity Properties

The far-infrared luminosity, in units of watts is given by

$$\mathrm{LFIR}=4\pi d^2\mathrm{FIR},$$

where the 40–120 μm flux, FIR, is

$$\mathrm{FIR}=1.26\times10^{-14}(2.58F_{60}+F_{100}),$$

where F_{60} and F_{100} are the flux densities in Janskys (Lonsdale *et al.* 1989). We have adopted $q_0=0.5$ and $H_0=50$ km s^{-1} Mpc^{-1} to derive the distance d.

Distributions of the observed far-infrared luminosities of UCM galaxies, superimposed on the *IRAS* minisurvey, UM, and Wasilewski samples are given in Figs. 5(a) to 5(c). The UCM luminosity extends over a range slightly larger than the *IRAS* minisurvey, on the low luminosity tail (log LFIR$=10.25L_\odot$). This difference is not balanced for lower luminosities, since the luminosity median of both samples differ by a factor of 3.7.

There is an excess of UM galaxies in the low-luminosity tail of the histogram with respect to the distribution of UCM galaxies. These UM objects with log LFIR $<8.75\ L_\odot$ are low-redshift bright galaxies which appear saturated in our survey plates. There are common boxes where the two samples peak, the UCM being clearly brighter. The luminosity medians of both samples are very close, 10.173 $L_\odot$ for UM and 10.186 $L_\odot$ for UCM.

The Wasilewski distribution is similar to the UM objective-prism survey. Also in this case the median luminosity, 10.222 $L_\odot$, is quite similar to the UCM one. In the four samples studied here, most of the galaxies are concentrated inside the boxes placed between 10.25 and 10.75 $L_\odot$. However the distributions of luminosities from objective-prism samples exhibit more similarity between them than with the *IRAS* minisurvey. Interestingly, the LFIRs median values for the objective-prism samples are close. However there is a remarkable difference: the blue surveys present a fraction of the low-luminosity objects without counterparts in the UCM sample.

On the basis of these comparisons, it seems unlikely that our optically-selected sample is the parent population of the *IRAS* minisurvey galaxies. The main reason is probably simple: the scale of FIR emitting regions is smaller in the UCM galaxies. In terms of dust heating mechanisms, this is an indication that the available supply of UV photons is less in the case of optically-selected galaxies than in FIR-selected galaxies. If the amplitude of the starburst is highly dependent upon the amount of molecular material available, it is likely that the UCM galaxies just have less intrinsic gas and dust than the *IRAS* minisurvey galaxies. On the other hand, as the far-infrared emission is mainly due to reradiation from dust heated by UV photons and stellar light, FIR properties are related to metal content in the sense that galaxies with lower metallicity are less efficient at creating dust than galaxies with normal metal content. Consequently, higher LFIR may correspond to higher metal content. This connection between LFIR and metallicity is consistent with the existence of a luminosity–metallicity relationship for the ELGs, which is in turn sim-

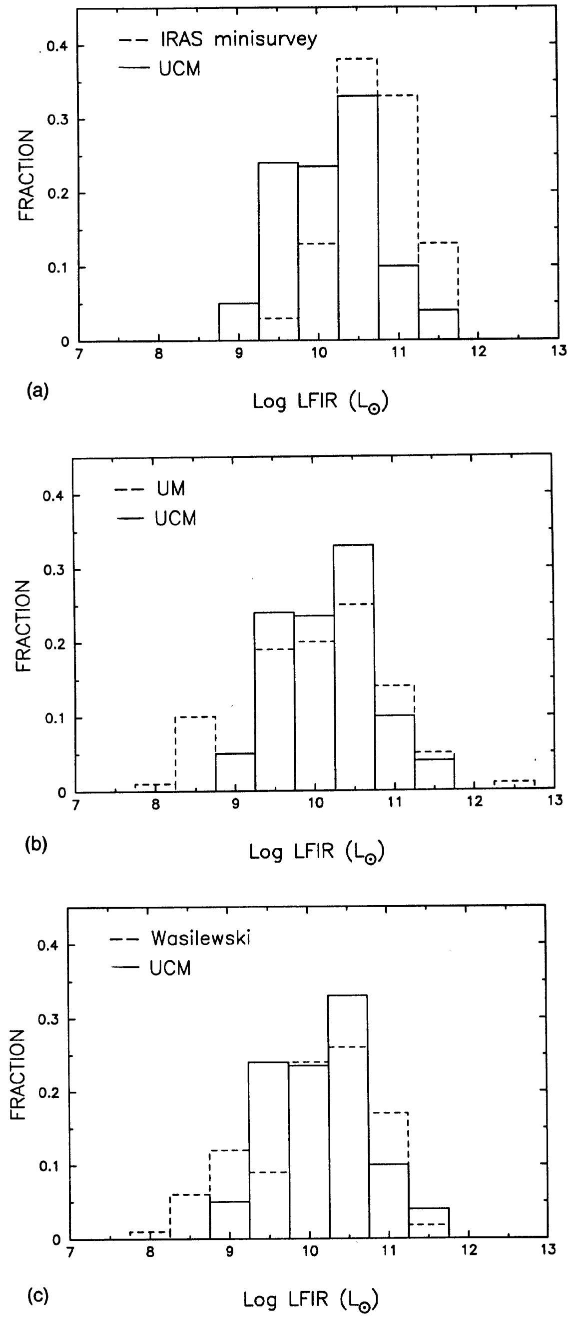

FIG. 5. Fractional distribution of UCM far-infrared luminosities (solid line) compared with those of (a) *IRAS* minisurvey, (b) UM, and (c) Wasilewski samples (dashed lines).

TABLE 2. Contributions of the three components to the UCM observed FIR fluxes.

NAME	d	b	s	σ
UCM0000+2140	0.05	0.83	0.13	0.05
UCM0003+2215	0.50	0.53	0.00	0.06
UCM0014+1748	0.35	0.50	0.15	0.01
UCM0018+2216	0.41	0.05	0.56	0.14
UCM0022+2049	0.61	0.35	0.05	0.01
UCM0037+2226	0.81	0.07	0.12	0.14
UCM0040+2312	0.90	0.00	0.11	0.04
UCM0043-0159	0.68	0.30	0.03	0.04
UCM0045+2206	0.48	0.33	0.20	0.03
UCM0047+2051	0.70	0.21	0.09	0.03
UCM0047+2413	0.42	0.59	0.00	0.02
UCM0047+2414	0.39	0.68	0.00	0.15
UCM0050+2114	0.22	0.75	0.03	0.02
UCM0051+2430	0.30	0.66	0.00	0.06
UCM0129+2109	0.54	0.46	0.00	0.09
UCM0142+2137	0.34	0.33	0.35	0.09
UCM0155+2507	0.43	0.61	0.00	0.09
UCM0157+2324	0.75	0.09	0.16	0.05
UCM0157+2413	0.50	0.50	0.00	0.02
UCM0159+2327	0.48	0.23	0.30	0.05
UCM1255+3125	0.40	0.12	0.50	0.05
UCM1256+2823	0.58	0.03	0.41	0.11
UCM1259+2755	0.39	0.30	0.31	0.02
UCM1259+2934	0.06	0.94	0.00	0.02
UCM1306+2937	0.61	0.27	0.13	0.15
UCM1308+2950	0.50	0.54	0.00	0.09
UCM1312+2954	0.38	0.17	0.44	0.05
UCM1312+3039	0.52	0.32	0.16	0.01
UCM1324+2650	0.31	0.39	0.30	0.00
UCM1428+2727	0.45	0.59	0.00	0.08
UCM1430+2947	0.57	0.10	0.35	0.13
UCM1442+2845	0.29	0.59	0.14	0.04
UCM1443+2714	0.30	0.16	0.55	0.01
UCM1447+2535	0.63	0.10	0.29	0.09
UCM1506+1924	0.34	0.66	0.00	O.02
UCM1513+2012	0.23	0.79	0.00	0.09
UCM1537+2506	0.22	0.62	0.16	0.01
UCM1557+1423	0.44	0.00	0.55	0.06
UCM1647+2950	0.54	0.25	0.20	0.04
UCM1648+2855	0.76	0.09	0.18	0.15
UCM1701+3131	0.48	0.54	0.00	0.09
UCM2238+2308	0.60	0.42	0.00	0.05
UCM2239+1959	0.14	0.61	0.27	0.13
UCM2250+2427	0.25	0.64	0.12	0.06
UCM2253+2219	0.13	0.59	0.29	0.01
UCM2256+2007	0.74	0.00	0.27	0.09
UCM2303+1856	0.00	0.96	0.04	0.01
UCM2316+2028	0.64	0.01	0.36	0.03
UCM2316+2457	0.42	0.58	0.00	0.01
UCM2317+2356	0.66	0.34	0.00	0.02
UCM2320+2428	0.51	0.00	0.47	0.10
UCM2321+2506	0.30	0.15	0.56	0.08
UCM2324+2448	0.87	0.00	0.13	0.03
UCM2325+1815	0.85	0.00	0.15	0.04
UCM2325+2208	0.63	0.37	0.00	0.03
UCM2325+2318	0.32	0.72	0.00	0.15
UCM2326+2435	0.62	0.36	0.02	0.04
UCM2327+2515	0.08	0.87	0.06	0.05

ilar to those found for disk galaxies (Salzer & MacAlpine 1988), in the sense that higher optical luminosity corresponds to higher metal content. The above results suggest that the metallicity of UCM galaxies may be lower than in *IRAS* minisurvey, however conclusive results must await the completion of the spectroscopic follow-up observation of the whole sample, which is in progress. A similar behavior is exhibited by the two other objective-prism samples. Moreover, there is strong evidence against the idea that the *IRAS* survey is equivalent to an objective prism survey sensitive to Hα emission, as was suggested by Bothun *et al.* (1989).

A more accurate comparison among the LFIRs distributions for the four samples has been carried out from nonparametric statistical methods. A test using the Wilcoxon method, with a significance level of 95%, leads to a probability p of 0.33 that UCM and UM samples come from the same distribution. The p values are 0.43, when the UCM and Wasilewski samples are taken into account, and finally, zero when the UCM and *IRAS* minisurvey are compared. This method yields results entirely consistent with those from the Kolmogorov–Smirnov test, which provide 0.24, 0.31, and 0.0 values, respectively, for the three couples. Both methods indicate that the best probability is obtained when the UCM and Wasilewski samples are compared.

6. THE THREE COMPONENT MODEL

We have selected 60 galaxies from the UCM sample with the highest quality *IRAS* fluxes which will be studied with more detail. We note that the derive results are not intended to provide information about the UCM sample at whole, from a statistical point of view. A three-component model proposed by Rowan-Robinson & Crawford (1989) has been applied. It postulated the FIR spectrum as (1) the mixture of the emissions of a normal "disk," modeled as a cirrus emission and warmer dust in the neighborhood of newly formed stars; (2) a "starburst" component, with a spectrum corresponding to a star-forming region embedded in dust clouds; and (3) a "Seyfert" component, whose spectrum is expected from re-emission by the dust surrounding a central power-law continuum source.

The assigned spectra of the components have been used to estimate their contributions to the observed FIR fluxes of the sample. When applied to the UCM sample, the weight observations have been taken into account in order to quantify the uncertainties in every band. Some of the UCM galaxies exhibit only upper limits in the 12 μm band, but the effect on the final results can be neglected considering its small relative weight. Table 2 displays the resulting values. Column 1 gives the UCM identification. Columns 2 to 4 list the contributed fraction of the components: d (normal disk), b (starburst), and s (Seyfert), with the computed errors.

A component has been considered predominant when its contribution is at least 60%. According to this criterion, the disk component has a predominant contribution in 27% of the UCM galaxies, while in 24% the starburst component is prevailing. There are eight UCM galaxies which have not been previously identified, either as galaxies or as emission-line galaxies. Only two objects, UCM 2321+2506 and UCM 0018+2216, exhibit FIR colors that could be interpreted as corresponding to Seyfert nuclei.

7. SUMMARY

In this paper we present an analysis of the FIR properties, based on *IRAS* data, of the UCM galaxies identified from an Hα objective-prism survey. Far-infrared fluxes obtained from the *IRAS* survey have been used to develop color–color diagrams of the UCM galaxies and a comparison sample of 546 galaxies, containing normal, starburst, and Seyfert galaxies. The diagrams, when interpreted from a simple two temperature model, suggest that a large fraction of the FIR radiation from the UCM galaxies is due to a warm-dust component that is heated by hot stars formed in a region of active star formation.

Comparison analyses from a statistical point of view were carried out among the UCM sample, *IRAS* minisurvey, and the UM and Wasilewski blue selected objective-prism samples. The UCM redshift distribution peaks around $z=0.025$, reflecting the coverage of the Coma supercluster. The redshift medians of all the considered samples are very close and confirm, as expected, that redshift distributions are indicators of the large structure more than any selection effects of the sample.

Far-infrared luminosities were determined for all the galaxies belonging to the mentioned samples and their distributions compared. Means and medians are close when the optical selected samples are taken into account, but there are significant differences when they are compared with *IRAS* minisurvey. Thus, the LFIR mean of the UCM sample is lower than the *IRAS* minisurvey one by a factor of about 3.7. Because LFIR may be related to the dust content and therefore to metallicity, we suggest that the UCM survey select galaxies with lower metallicity.

Nonparametric tests of the LFIRs based on the Wilcoxon and Kolmogorov–Smirnov methods provide the best p value for the UCM and Wasilewski samples and discard the *IRAS* minisurvey as a parent population of the UCM galaxies.

Finally, the UCM galaxies with higher qualities *IRAS* fluxes were analyzed for a three component model which provides the fractions of the normal disk, starburst, and Seyfert components in the observed fluxes. In this way the contribution of each component in the galaxy subsample has been pointed out. Nearly all the objects exhibit FIR emission that can be interpreted as powered by thermal mechanisms. Only UCM 2321+2506 and UCM 0018+2216 can be considered as Seyfert candidates.

We wish to thank the staff at Rutherford Appleton Laboratory for their friendly assistance and hospitality during the visit of J.G. in November 1991. This work was supported in part by the Spanish "Programa Sectorial de Promoción General del Conocimiento" under Grant No. PB89-124.

REFERENCES

Balzano, X. 1983, ApJ, 268, 602

Bothun, G. D., Halpern, J. P., Lonsdale, C. J., & Impey, C. 1989, ApJS, 70, 271

Carico, D. P., Soifer, B. T., Beichman, C., Elias, J. H., Mathews, K., & Neugebauer, G. 1986, AJ, 92, 1254

Dahari, O., & de Robertis, M. 1988, ApJS, 67, 249

Dennefeld, M. Karoji, H., & Belfort, P. 1985, in Star-Forming Dwarf Galaxies and Related Objects, edited by D. Kunth, T. X. Thuan, and J. Tran, p. 351
Désert, F. X. 1986, in Light on Dark Matter, edited by F. P. Israel, p. 213
Devreux, N. A., Becklin, E. E., & Scoville, N. 1987, ApJ, 312, 529
Dreyer, J. L. 1888, Mem. RAS 49
Geller, M. J. Beers, T. C., Huchra, J. P., & Bothun, G. D. 1988, AJ, 89, 319
Green, R. F., Smidt, M., & Liebert, J. 1986, ApJS, 6, 305
Holmberg, E. 1937, Annals Obs. Lund, 6
Karachentsev, I. D. 1972, A Catalog of Isolated Pairs of Galaxies in the North Hemisphere, Astrofiz. Issled. Izu, Spets. Astrofiz. 7, 3
Kazarian, M. A., & Kazarian, E. S. 1980, Afz, 16, 17
Klein, U., Wielebinski, R., & Thuan, T. X. 1984, A&A, 141, 241
Kunth, D., & Sargent, W. L. W. 1983, ApJ, 273, 81
Lonsdale, C. J., Helou, G., Good, J. C., & Rice, W. 1989, Catalogued Galaxies and Quasars in the IRAS Survey (Jet Propulsion Laboratory, Pasadena)
MacAlpine, G. M., & Williams, G. A. 1981, ApJS, 45, 113
Markarian, B. E., & Lipovetskii, V. A. 1971, Afz, 7, 511
Markarian, B. E., & Lipovetskii, V. A. 1972, Afz, 8, 155
Markarian, B. E., & Lipovetskii, V. A. 1973, Afz, 9, 487
Markarian, B. E., & Lipovetskii, V. A. 1974, Afz, 10, 307
Markarian, B. E., & Lipovetskii, V. A. 1979, Afz, 15, 201
McBreen, B., Fazio, G. G., & Jaffe, D. T. 1982, ApJ, 254, 126
Natta A., & Panagia, N. 1976, A&A, 50, 191
Nilson, P. 1973, Uppsala General Catalogue of Galaxies (Royal Society of Sciences of Uppsala, Uppsala)
Paturel, G., Fouqué, P., Bottinelli, L., & Gouguenheim, L. 1989, A&AS, 80, 299
Pesch, P., Sanduleak, N., & Stephenson, C. B. 1991, ApJS, 76, 1041
Rego, M., Zamorano, J., & González-Riestra, R. 1989, A&AS, 62, 173
Reiz, A. 1941, Annals Obs. Lund, 9
Rowan-Robinson, M., & Crawford, J. 1989, MNRAS, 238, 523
Salzer, J. J., & MacAlpine, G. M. 1988, AJ, 96, 1192
Sekiguchi, K. 1987, ApJ, 316, 145
Takase, B., & Miyauchi-Isobe, N. 1991, PNAO Japan, 2, 7
Thronson, H. A., & Price, S. D. 1982, ApJ, 87, 288
Veron-Cetti, M. P., & Veron, P. 1991, A Catalogue of Quasars and Active Nuclei (European Southern Observatory, Garching)
Vorontsov-Velyaminov, B. A., & Krasnogorskaja, A. A. 1962, Morphological Catalog of Galaxies (Moscow State University, Moscow)
Wasilewski, A. J. 1983, ApJ, 272, 68
Xu, C., & De Zotti, G. 1989, A&A, 225, 12
Zamorano, J., Rego, M., & González-Riestra, R. 1990, Ap&SS, 170, 353
Zotti, G., Franceschini, A., & Danese, L. 1988, A&A, 196, 59
Zwicky, F., & Herzog, E. 1963, Catalogue of Galaxies and Cluster of Galaxies (California Institute of Technology, Pasadena)